THE JOURNAL OF PHYSICAL CHEMISTRY B

Article

pubs.acs.org/JPCB

Nonmonotonic Rayleigh-Taylor Instabilities Driven by Gas−Liquid CO_2 Chemisorption

C. Wylock,* A. Rednikov, B. Haut, and P. Colinet*

Université Libre de Bruxelles (ULB), Transfers, Interfaces and Processes (TIPs), av. F.D. Roosevelt 50, CP 165/67, 1050 Brussels, Belgium

Supporting Information

ABSTRACT: Density variations induced by gas absorption in reactive aqueous solutions often trigger buoyancy-induced motions, generally in the form of plumes monotonically sinking into the bulk liquid and enhancing the absorption rate. Here, we contrast two types of CO_2-absorbing alkaline solutions, studying their dynamics inside a vertical Hele-Shaw cell by interferometry. While the first one indeed behaves as expected, the second one leads to a quite unusual oscillatory (phase-slipping) dynamics of convective plumes, which moreover does not lead to a significant transfer enhancement. Thanks to a simplified model of momentum and species transport, we show that this particular dynamics is related to a nonmonotonic density stratification, resulting in a stagnant layer close to the interface. Conditions for this to occur are highlighted in terms of the ratios of species' diffusivities and their contribution to density, a classification deemed to be useful for optimizing chemisorption (e.g., for CO_2 capture or sequestration) processes.

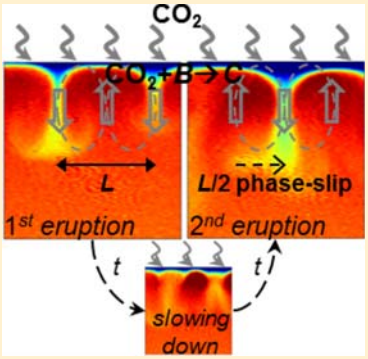

INTRODUCTION

Rayleigh-Taylor instabilities (RTI) are buoyancy-induced flows developing from small fluctuations whenever a heavier fluid layer lies on top of a lighter one in the field of gravity.[1−3] They are observed in a wide range of fields, such as geology,[4] hydrology,[5] astrophysics,[6] and even plasma science.[7] Whatever the origin of density gradients in the fluids, RTI are generally expected to occur in the form of plumes monotonically sinking into the bulk liquid, hence, driving an intense mixing and enhancing the rate of heat and mass transfer. For this reason, RTI are also increasingly studied nowadays in the framework of carbon dioxide (CO_2) sequestration in deep saline aquifers,[8−10] a process for which mixing is expected to add up to the effect of chemical reactions in boosting the overall efficiency.

Figure 1, explained in more detail later on, presents experimental results obtained when gaseous CO_2 is absorbed in two different initially quiescent aqueous solutions, in otherwise similar conditions. Figure 1a−f is obtained when absorbing gaseous CO_2 into an aqueous solution of monoethanolamine (MEA, 870 mol/m^3, hereafter solution 1). It illustrates the classical scenario where denser plumes monotonically finger downward. In contrast, Figure 1g−l, obtained for the absorption of CO_2 in an aqueous solution of sodium bicarbonate ($NaHCO_3$, 790 mol/m^3) and sodium carbonate (Na_2CO_3, 625 mol/m^3), shows a quite unusual behavior. Hereafter, this solution will be referred to as solution 2. Indeed, instead of plunging deep inside the fresh liquid, plumes here appear to slow down at some depth, soften, and almost vanish. Meanwhile, a second generation of plumes appears in between the primary ones, eventually repeating the same scenario and leading to an oscillatory dynamics (this is more easily seen in some of the movies included as Supporting Information). Note that this behavior is observed in solution 2 for any pair of the initial $NaHCO_3$ and Na_2CO_3 concentrations used. In most cases, the spatial wavenumber of the plume pattern is comprised between 1.5 and 3 mm^{-1} and tends to increase for successive plume generations. In addition, it is observed that the period between the first and the second generations is usually close to 2 min and that this time-delay between successive generations tends to increase with time.

The goal of the present paper is therefore to understand the physicochemical mechanisms at the origin of such a particular dynamics and, more generally, to propose a classification of possible RTI dynamics occurring during the absorption of CO_2 in a liquid solution, on the basis of the relevant properties of the CO_2-absorbing solution at hand. In addition, it is also crucial to quantify the impact of such flows on the enhancement of the global absorption/conversion rate. As it will be seen hereafter, the density profile prior to instability, monotonic for solution 1 and nonmonotonic for solution 2 (see top of Figure 1), essentially determines the overall dynamics. Note in this respect that the present analysis goes beyond recent works concerned with miscible reactive two-liquid systems.[11−13] Indeed, these authors do not evidence any oscillatory dynamics in the nonlinear regime, as we do here both experimentally and on the basis of a simplified model of the CO_2 chemisorption process.

The experimental sequences depicted in Figure 1 have been recorded in a vertical Hele-Shaw cell (two glass plates separated by a gap of thickness 0.5 mm for solution 1 and 1.9 mm for solution 2, width 30 mm, liquid filling the gap up to a height of

Received: July 14, 2014
Revised: August 29, 2014

   dx.doi.org/10.1021/jp5070038 | J. Phys. Chem. B XXXX, XXX, XXX−XXX

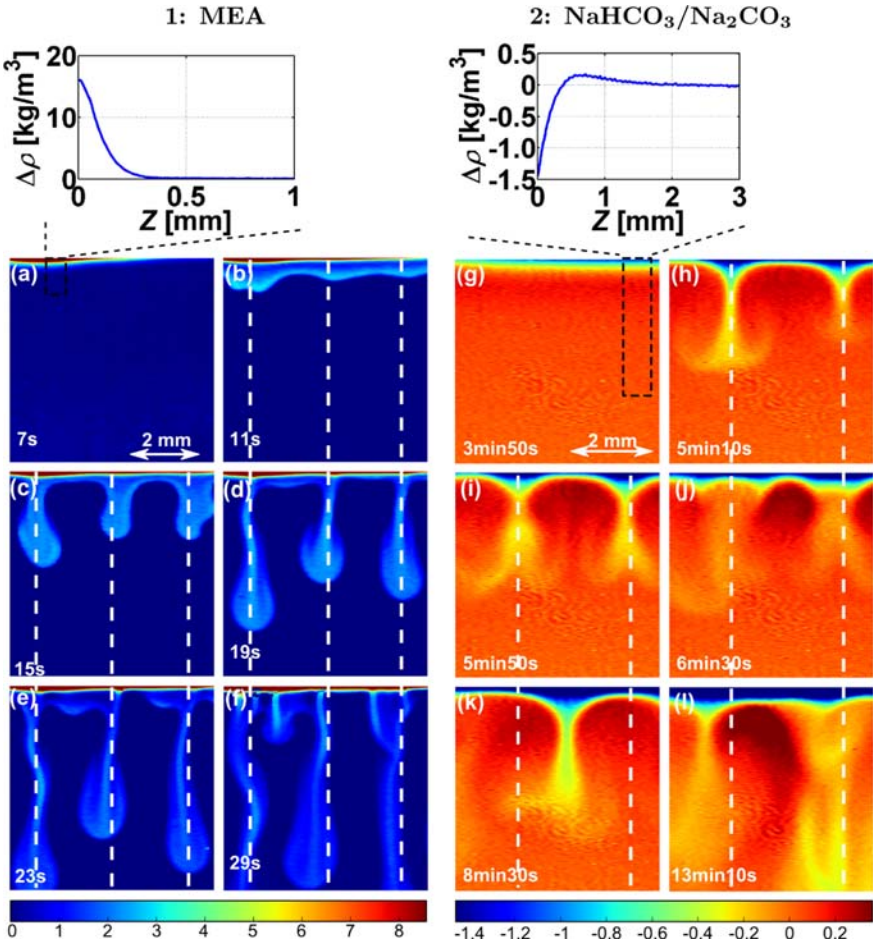

Figure 1. Experimental density variation (DV) fields in the liquid at various times during CO_2 absorption in solution 1 (a–f) and in solution 2 (g–l). Shown above each sequence are horizontally averaged DV profiles computed for (a) and (g), that is, before instability onset. Z is the depth into the liquid (i.e., down vertical coordinate) from the interface (where $Z = 0$). Dashed vertical lines indicate the position of initial plumes.

50 mm), as often used to study RTI, as this configuration enables quasi-bidimensional visualization while at the same time mimicking porous media flows.[14] We here focus on the liquid phase behavior just underneath the horizontal gas–liquid interface (located on top of each image). Using a Mach–Zehnder interferometer (MZI) and thanks to the procedure described in Wylock et al.,[15] the refractive index variation (RIV) field induced in the liquid by the CO_2 absorption can be extracted. For both solutions, a calibration has been carried out and a linear correlation has been found between RIV and density variation $\Delta\rho$. Such a device therefore enables following the spatiotemporal dynamics of the density variations (DV).

Besides what was already said above in relation with Figure 1, another important observation is that the plumes are formed about 1 mm below the interface for solution 2, while they appear right at the interface for solution 1. This fact, which will be further examined numerically in what follows, suggests that the key to understand the different dynamical regimes lies in the different DV shapes before instability sets in (see the top of Figure 1). Indeed, for solution 1, the maximum DV is located at the interface and the DV decreases monotonically with the depth Z. For solution 2, the DV is minimum at the interface. It first increases with Z, reaching a positive maximum at 0.75 mm below the interface and then starts to decrease. In order to explain this and to highlight further differences between solutions 1 and 2, we now turn to a simplified (yet realistic) model of the reaction–diffusion–convection dynamics. It is worth mentioning, however, that the goal of the present study is not an exact modeling of the experiments, but rather to extract the essence of the phenomena with the help of a simple model.

MATHEMATICAL MODELING

Basic Hypotheses. For both considered solutions, the reactions are rather fast as compared to the species transport (see Aboudheir et al.[16] for solution 1 and Vas Bhat et al.[17] for solution 2). The reactions are then confined to a thin liquid layer at the interface, beyond which CO_2 is nearly depleted. This permits the simplification of the reaction scheme by considering an instantaneous reaction $A + B \rightarrow C$ taking place only at the gas–liquid interface. Such an approach, which is described in more detail in Supporting Information, is commonly used for gas absorption, coupled with fast reactions.[18,19] It is deemed to be quite a reasonable one in our case, the actual reaction zone being much thinner than the diffusive boundary layer at the instability onset. In our model, A corresponds to CO_2 (not penetrating in the liquid), whereas B and C are the reactant and the product transported from/to the bulk of the liquid, respectively. Let $[B]$ and $[C]$ be the corresponding concentration fields. Before the gas–liquid absorption begins, these are equal to the initial (homogeneous) concentrations $[B]_0$ and $[C]_0$, respectively.

dx.doi.org/10.1021/jp5070038 | J. Phys. Chem. B XXXX, XXX, XXX–XXX

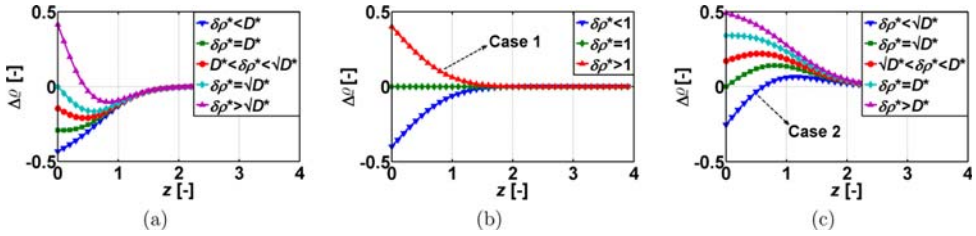

Figure 2. Dimensionless DV profile shapes (here with $\Delta\rho_{ref} = \partial_{[B]}\rho[B]_0$, i.e., $\zeta = 1$) for $D^* < 1$ (a), $D^* = 1$ (b), and $D^* > 1$ (c). To define, all profiles are drawn at the same dimensionless time $t = 0.25$.

Due to the instantaneous character of the reaction, B is totally depleted at the interface, with $[B] = 0$ at this point. Before the instability onset, B and C are transported only by diffusion. For the configuration used in the experiments, the DV profile before the onset can be approached by a one-dimensional (1-D) model. We shall work in terms of the dimensionless concentrations $b = [B]/[B]_0$ and $c = [C]/[B]_0$ and define $c_0 = [C]_0/[B]_0$. In general, the species B and C have different diffusion coefficients and contribute differently to the density ρ (assumed to vary linearly with $[B]$ and $[C]$). Let $D^* = \mathbb{D}_C/\mathbb{D}_B$ and $\delta\rho^* = \partial_{[C]}\rho/\partial_{[B]}\rho$ be the diffusivity and density contribution ratios, respectively.

The dimensionless spatial coordinates and time t are defined using the scales l_{ref} and $t_{ref} = l_{ref}^2/\mathbb{D}_B$, respectively, where l_{ref} will be specified later on.

One-Dimensional Reference Profiles. Considering the model hypotheses, the dimensionless 1-D diffusion equations read

$$\partial_t b = \partial_{zz} b \tag{1}$$

$$\partial_t c = D^* \partial_{zz} c \tag{2}$$

At the interface ($z = 0$), the complete depletion of B (due to the instantaneous interfacial reaction) and a production of C equal to the consumption of B are considered (see Supporting Information):

$$b = 0 \tag{3}$$

$$D^* \partial_z c = -\partial_z b \tag{4}$$

At $t = 0$, as well as for $z \to +\infty$, we specify

$$b = 1 \tag{5}$$

$$c = c_0 \tag{6}$$

The solution of the problems 1−6 is

$$b(z, t) = \mathrm{erf}\left(\frac{z}{2\sqrt{t}}\right) \tag{7}$$

$$c(z, t) = c_0 + \frac{1}{\sqrt{D^*}}\mathrm{erfc}\left(\frac{z}{2\sqrt{D^* t}}\right) \tag{8}$$

yielding the dimensionless concentration profiles of B and C in the reference state, the stability of which will be considered in the next section.

The dimensionless DV profile is calculated as

$$\Delta\rho = \zeta((b - 1) + \delta\rho^*(c - c_0)) \tag{9}$$

where $\zeta = \partial_{[B]}\rho[B]_0/\Delta\rho_{ref}$ is a constant coefficient, in which $\Delta\rho_{ref}$ is a dimensional reference DV value to be specified. Hence, we have

$$\Delta\rho(z, t) = \zeta\left(\frac{\delta\rho^*}{\sqrt{D^*}}\,\mathrm{erfc}\left(\frac{z}{2\sqrt{D^* t}}\right) - \mathrm{erfc}\left(\frac{z}{2\sqrt{t}}\right)\right) \tag{10}$$

showing that the DV profile is self-similar and that its shape is controlled by the values of D^* and $\delta\rho^*$. Figure 2 classifies the different shapes found from this expression, depending on the values of these two parameters.

In particular, Figure 2 shows that the nonmonotonic DV profiles observed for solution 2 occur when $D^* > 1$ and $\delta\rho^* < (D^*)^{1/2}$, which indeed turns out to be the case (from the physicochemical parameters deduced for solution 2,[15] it is found that $D^* \approx 1.25$, $\delta\rho^* \approx 0.9$). In contrast, it has been estimated that $D^* \approx 1$ and $\delta\rho^* \approx 2.2$ for solution 1 (from MZI experiment analysis). The profile shapes predicted in Figure 2 are therefore in qualitative agreement with those obtained experimentally. Note that besides the two cases 1 and 2 studied here, several other DV shapes can, in principle, be induced, depending on the values of D^* and $\delta\rho^*$.

Momentum and Mass Transport Model. In order to analyze the RTI dynamics, we consider a two-dimensional (2-D) formulation of the liquid phase flow inside the Hele-Shaw cell, using the Boussinesq approximation together with an effective (gap-averaged) Navier−Stokes−Darcy[20−23] equation for the velocity field. It should be stressed here that the balance equations for B and C do not include any reaction terms since the reaction is considered to take place at the interface and not in the bulk (see above and in the Supporting Information). The dimensionless continuity, momentum, and species transport equations are thus written as

$$\nabla\cdot\mathbf{u} = 0 \tag{11}$$

$$\frac{1}{\mathrm{Sc}}\left(\partial_t\mathbf{u} + \frac{6}{5}\mathbf{u}\cdot\nabla\mathbf{u}\right) = -\nabla p + \nabla^2\mathbf{u} - \frac{u}{\mathrm{Da}} + \mathrm{Ra}\Delta\varrho e_z \tag{12}$$

$$\partial_t b + \mathbf{u}\cdot\nabla b = \nabla^2 b \tag{13}$$

$$\partial_t c + \mathbf{u}\cdot\nabla c = D^*\nabla^2 c \tag{14}$$

where $\nabla = (\partial_x, \partial_z)$, x and z are the horizontal and vertical dimensionless coordinates, the latter directed downward as before with $\boldsymbol{e}_z$ the corresponding unit vector, $\mathbf{u} = (u,v)$, and p are the velocity and pressure fields adimensionalized with $\mathbb{D}_B/l_{ref}$ and $\mu\mathbb{D}_B/l_{ref}^2$, respectively, μ is the dynamic viscosity and $\Delta\rho$ is given by the earlier expression. Ra, Da, and Sc are the Rayleigh, Schmidt and Darcy numbers, respectively, defined as

$$\mathrm{Ra} = \frac{\Delta\rho_{ref} g l_{ref}^3}{\mu\mathbb{D}_B} \tag{15}$$

dx.doi.org/10.1021/jp5070038 | J. Phys. Chem. B XXXX, XXX, XXX−XXX

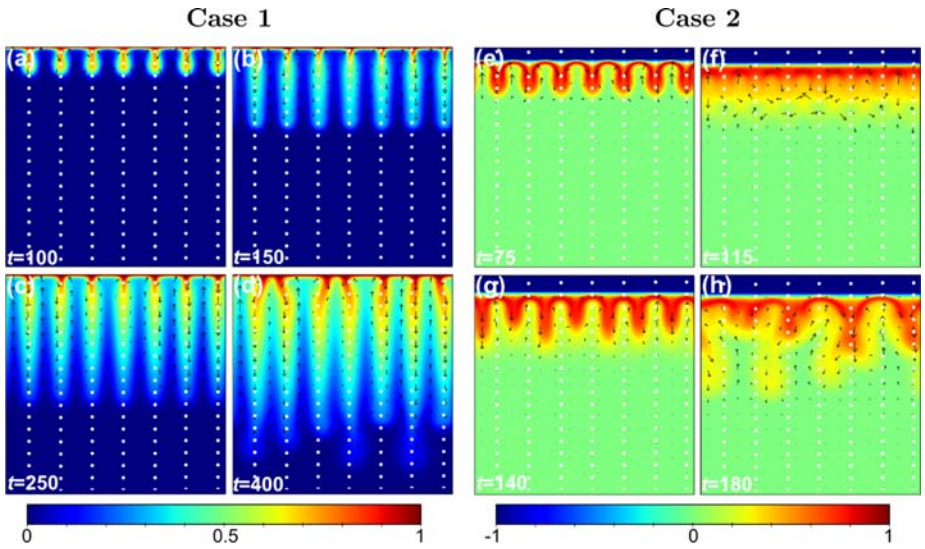

Figure 3. Simulated dimensionless DV fields (color) and velocity fields (arrows) at various dimensionless times for case 1 (a–d) and case 2 (e–h).

$$\mathrm{Sc} = \frac{\mu}{\rho_0 \mathbb{D}_B} \tag{16}$$

$$\mathrm{Da} = \frac{h^2}{12 l_{ref}^2} \tag{17}$$

where ρ_0 is the initial liquid density and h is the distance between the two plates of the Hele-Shaw cell. Note that eq 12 differs from the Navier–Stokes equation by the presence of the Darcy term as well as by a coefficient 6/5 multiplying the nonlinear term, as shown to be applicable for such kind of 2-D description of Hele-Shaw flows.[21]

At the top boundary (the interface, $z = 0$), the conditions for b and c, already defined by eqs 3 and 4, are complemented by the conditions applicable to a motionless impermeable stress-free interface:

$$v = 0 \tag{18}$$

$$\partial_z u + \partial_x v = 0 \tag{19}$$

It is worth mentioning that possible solutal and thermal (CO_2 chemisorption is slightly exothermic) Marangoni effects at this boundary are not considered here, our intention being to capture the essence with a model as minimalistic as possible. Moreover, we do not observe any clear sign of a Marangoni-type convection in experiments with solution 2. In particular, the interfacial stagnant layer of this solution remains largely motionless during the whole process, even after the instability onset. Admittedly though, this argument does not hold for solution 1, where the interfacial layer is not stagnant. Yet, solution 1 is not studied in such detail here, as it merely serves as an illustration of "classical" plume dynamics with which we contrast the unusual dynamics of solution 2.

The bottom boundary is set as an open boundary regarding the flow and the species transport, characterized by the following conditions:

$$\partial_z u + \partial_x v = 0 \tag{20}$$

$$-p + 2\partial_z v = 0 \tag{21}$$

$$\partial_z b = 0 \tag{22}$$

$$\partial_z c = 0 \tag{23}$$

The horizontal dimension is treated by means of periodic boundary conditions applied between the left and right boundaries.

Clearly, the 1-D diffusion profiles found above correspond to a particular solution (the reference, or rest state solution) of this general boundary-value problem, with $\mathbf{u} = 0$ and p balancing the buoyancy term of eq 12. In order to explore its stability with respect to hydrodynamic disturbances, we impose as initial conditions either a numerical or an imposed controlled noise (see below), superposed to initial fields $b = 1$, $c = c_0$, and $u = v = 0$. Note finally that for the so far undefined reference values, we choose $\Delta\rho_{ref} = \Delta\rho_{max}$, which is the maximum of the dimensional DV in the reference state, and l_{ref} is selected such that Ra = 1.

RESULTS AND DISCUSSION

Flow Simulations. Two simulation cases are investigated, namely, cases 1 and 2. The parameters D^* and $\delta\rho^*$ for cases 1 and 2 are selected such as to roughly correspond to the DV profile shapes experimentally observed in solutions 1 (Figure 2b) and 2 (Figure 2c), respectively. From the physicochemical parameters for solution 2 (see above), the following values are used for case 2: $D^* = 1.25$, $\delta\rho^* = 0.9$. We then also obtain $\zeta = 68.5$, $l_{ref} = 1.4 \times 10^{-4}$ m, and Da = 15.15. In order to have for simplicity the same ζ for cases 1 and 2, the following values are then deduced to represent case 1: $D^* = 1$ and $\delta\rho^* = 1.014$. For the other parameters, we use Sc = 500, Da = 15.15 (used for both cases, again for simplicity), Ra = 1 (from the definition of l_{ref}), and $c_0 = 0$. The dimensionless length and height of the computational domain are taken to be 250. The problem is numerically solved by a finite element method using COMSOL Multiphysics.

As expected, given the density profiles considered, a Rayleigh-Taylor-like dynamics is observed for both cases 1 and 2. Importantly, when simulations are ran without imposing a controlled noise (i.e., when the perturbations originate from the numerical noise only), there are 7 plumes that are most often observed in our computational domain at the instability onset for both cases. However, further evolutions might be different between different runs of the same simulation since

dx.doi.org/10.1021/jp5070038 | J. Phys. Chem. B XXXX, XXX, XXX–XXX

the system is highly unstable and the numerical noise is randomly distributed. In order to trigger RTI from a controlled perturbed state, a noise function in the form $A_N \exp(-F_N z) \sin(-F_N x)$ is superimposed on the initial field of b, with $A_N = 10^{-8}$ the noise amplitude and $F_N = 14\pi/250$ the noise spatial frequency (7 wavelengths in the domain).

The simulation results obtained for both cases are shown in Figure 3, where the DV fields are presented at various times after the instability onset. It is observed that the simulation results are in qualitative agreement with the experimental ones. In case 1, the plumes are formed at the interface and sink monotonically. In the case 2, a first generation of plumes are formed at a small finite distance from the interface (actually where $\Delta\rho$ has its maximum). They seem to soften down a short time later, and it is clearly observed that a second generation of plumes is formed in between the previous ones (i.e., the phase of the periodic disturbance slips by half a wavelength). By examining the velocity field (see the movies provided as Supporting Information), it appears that the liquid velocity in the zones where the plumes are sinking slows down during the softening phase, before being reversed (see Figure 3e–g). The zones where the liquid is flowing downward during the first generation of plumes become the zones where the liquid is flowing upward at the second generation. For longer times than those presented in Figure 3d,h for cases 1 and 2, respectively, the plumes tend to move laterally and to merge for both cases, reducing the spatial frequency of the plume pattern, which is also in agreement with experiments (though such coarsening is eventually observed after longer times than those presented in Figure 1).

By further analyzing the simulation results, it clearly appears that the difference in dynamics between cases 1 and 2 is linked to the existence in case 2 of a quiescent zone near the interface, where the density stratification is stable (see blue zone in Figure 3e–h). In both cases, however, right after the plumes formation, the rate of the interfacial chemical reaction is enhanced at horizontal locations where the liquid flows upward (i.e., in between the plumes) because of the resulting convective supply of fresh reactant B. One could therefore expect a density increase there in both cases 1 and 2, as both B and C contribute positively to the density. While in case 1, convection along the interface is sufficiently strong to transport this interplume density excess laterally toward the falling plumes (hence, sustaining this falling motion), this does not appear to be the case for case 2, where a significant excess of density remains in between the initial plumes, in the zone of transition between the quiescent layer and the convective zone. At the same height, it can be seen from Figure 3e that the density at the plumes is comparatively lower. After a certain time, this density field configuration is able to slow down and even reverse the flow, triggering a second generation of plumes in between the initial ones, and hence, explaining this particular phase-slipping dynamics.

Linear Stability Analysis. To further investigate the particular nonmonotonic RTI dynamics observed in case 2 and contrast it with case 1, we use a frozen-time linear stability analysis to calculate the complex growth rates $\sigma + i\omega$ of spatially periodic normal modes $\propto \exp(ikx)$, perturbing the horizontally uniform (reference) state $\mathbf{u} = 0$, $b = b(t,z)$, $c = c(t,z)$. We consider a moment of time right before the instability onset becomes manifest in the simulations (at $t = 80$ for case 1 and $t = 50$ for case 2). Here k is the wavenumber. It is made dimensionless with l_{ref}^{-1}, whereas σ and ω are scaled by t_{ref}^{-1}. The results for cases 1 and 2 are shown in Figure 4. We see that the system is strongly linearly unstable (the maximal values of σ are

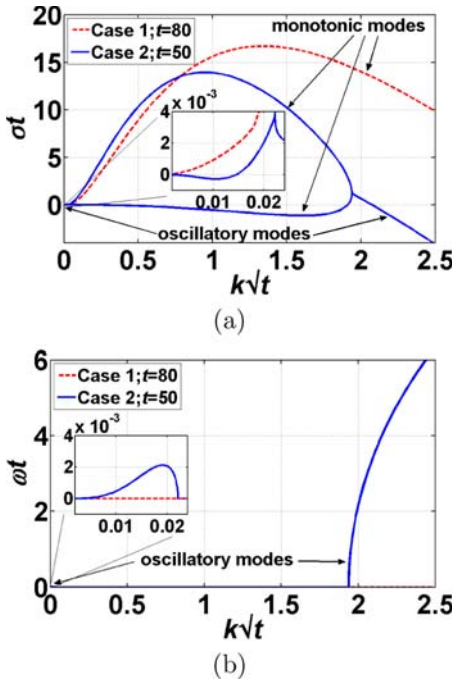

Figure 4. Dimensionless growth rate (a) and frequency (b) of small perturbations vs the wavenumber right before a manifest instability onset in 2-D simulations.

positive and significantly greater than t^{-1}) already well before the plume eruption actually occurs. The reason for why it does not occur earlier can be attributed to the fact that the initial noise needs time to get sufficiently amplified. We note that the maximum growth rate can be verified to correspond to about 6 wavelengths (plumes) in our computational domain for both case 1 and case 2. As expected, this is reasonably well in agreement with the number of plumes (generally 7) initially erupting in the simulations starting from the numerical noise.

Arguably the most remarkable result of Figure 4 is the presence, rather unexpected for problems of this kind, of oscillatory modes ($\omega \neq 0$) in case 2. It is worth mentioning that a similar diagram has been obtained for a different setup (miscible liquid layers) in Trevelyan et al.[13] However, these authors did not observe oscillatory dynamics in their nonlinear analysis of the corresponding regimes. On the other hand, case 1 remains "usual" in this regard, with only monotonic modes throughout. In case 2, even though the most unstable modes are still monotonic, their nonlinear interactions are likely to involve higher-wavenumber oscillatory ones, damped or (slightly) amplified. It is apparently such an intrinsic mechanism of oscillations present in case 2 that is at the core of the observed (both experimentally and numerically) peculiarities of the initial plume eruption discussed earlier. Curiously enough, even though this is not of direct relevance to the instability outbreak observed here, the linear stability analysis (frozen-time) reveals that, in case 2, the first unstable modes appearing at smaller t values are all oscillatory. It is just later, as t is increased, that they turn monotonic at the most unstable interval of k, as in Figure 4.

Transfer Rate. Finally, another remarkable difference between case 1 and case 2 concerns the impact of convection

dx.doi.org/10.1021/jp5070038 | J. Phys. Chem. B XXXX, XXX, XXX–XXX

on the interfacial mass transfer rate. The already-mentioned existence of a stably stratified quiescent layer (growing with time) near the interface in case 2 must indeed modify considerably the mass transfer dynamics as compared to case 1, in which RTI induce considerable liquid motion/mixing close to the interface. To assess its influence, a dimensionless mass transfer rate J is evaluated by integrating $-\partial_z b$ along the interface boundary in the computational domain for both cases and compared to the corresponding result in the absence of convection (i.e., when $\mathbf{u} = 0$).

The results, represented in Figure 5, clearly show that the transfer rate is significantly enhanced by the RTI for case 1,

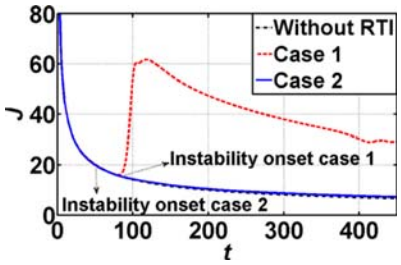

Figure 5. Dimensionless integral mass transfer rates vs time for cases 1 and 2 and a comparison with the 1-D diffusional regime (without RTI) with $D^* = 1$.

whereas it is just very slightly enhanced for case 2. This is indeed due to the fact that, in case 2, mass transport in the quiescent interfacial region remains mainly diffusive. This result highlights that the RTI development does not necessarily lead to a significant mass transport enhancement, contrary to what is commonly expected.

CONCLUSIONS AND PERSPECTIVES

We have here considered CO_2 absorption in an initially quiescent and horizontal aqueous solution, where it is consumed in a fast chemical reaction. Depending on the ratios of species' diffusivities and their contribution to density, the density stratification generated by the CO_2 absorption may in some cases turn out to be nonmonotonic, with a stable region near the interface, which has several important consequences: stagnant layer at the interface, oscillatory RTI dynamics, and very weak mass transfer enhancement after the RTI appearance, contrary to what happens for a monotonically unstable density stratification. Density profiles observed experimentally before the RTI onset can be predicted by a rather simple 1-D model of the diffusive transport of the reactant and the product, and the observed RTI dynamics can be reproduced by coupling in a 2-D formulation the species transport to the momentum transport, described by a Navier–Stokes–Darcy model (adapted to Hele-Shaw cells or porous media). A promising perspective would be to identify solutions corresponding to the nonmonotonic profiles of Figure 2a and to study their RTI dynamics. We hope that the present work will stimulate further research both on the fundamentals of gas chemisorption and on applications in CO_2 capture and storage technologies (including milli- or microfluidic devices), together with more classical processes of the chemical industry.

ASSOCIATED CONTENT

Supporting Information

The rationale behind the simplified chemical reaction model (instantaneous interfacial chemical reaction) used in the present study is elaborated. Animations of the time evolution of the experimental DV fields for solutions 1 and 2 (as presented in Figure 1), another aqueous solution $NaHCO_3$ (519 mol/m^3) and Na_2CO_3 (617 mol/m^3), and time evolution of the simulated DV for cases 1 and 2 (as presented in Figure 3) are also available as movies. This material is available free of charge via the Internet at http://pubs.acs.org.

AUTHOR INFORMATION

Corresponding Authors

*E-mail: cwylock@ulb.ac.be.
*E-mail: pcolinet@ulb.ac.be.

Notes

The authors declare no competing financial interest.

ACKNOWLEDGMENTS

The authors are thankful to Prof. A. De Wit and her team for helpful discussions. C.W. and P.C. are, respectively, a Postdoctoral Researcher and a Senior Research Associate of the Fonds de la Recherche Scientifique-FNRS, which is gratefully acknowledged for its support. The authors also acknowledge financial support of BELSPO and ESA via the PRODEX programme. This study is also related to the activity of the European network action COST MP1106 "Smart and green interfaces - from single bubbles and drops to industrial, environmental and biomedical applications".

REFERENCES

(1) Rayleigh, J. W. S. Investigation of the character of the equilibrium of an incompressible heavy fluid of variable density. *Proc. London Math. Soc.* **1883**, *14*, 170–177.
(2) Sharp, D. H. An overview of Rayleigh-Taylor instability. *Physica D* **1984**, *12*, 3–10.
(3) Kull, H. J. Theory of the Rayleigh-Taylor instability. *Phys. Rep.* **1991**, *206*, 197–325.
(4) Gerya, T. A.; Yuen, D. A. Rayleigh-Taylor instabilities from hydration and melting propel "cold plumes" at subduction zones. *Earth Planet Sci. Lett.* **2003**, *212*, 47–62.
(5) Wooding, R. A.; Tyler, S. W.; White, I.; Anderson, P. Convection in groundwater below an evaporating salt lake: 2. Evolution of fingers or plumes. *Water Resour. Res.* **1997**, *33*, 1219–1228.
(6) Wang, C. Y.; Chevalier, R. A. Instabilities and clumping in type Ia supernova remnants. *Astrophys. J.* **2001**, *549*, 1119–1134.
(7) Hoshoudy, G. A. Quantum effects on the Rayleigh-Taylor instability of stratified fluid/plasma through porous media. *Phys. Lett. A* **2009**, *373*, 2560–2567.
(8) Riaz, A.; Hesse, M.; Tchelepi, H. A.; Orr, F. M. Onset of convection in a gravitationally unstable diffusive boundary layer in porous media. *J. Fluid Mech.* **2006**, *548*, 87–111.
(9) Javaheri, M.; Abedi, J.; Hassanzadeh, H. Linear stability analysis of double-diffusive convection in porous media, with application to geological storage of CO_2. *Transp. Porous Media* **2010**, *84*, 441–456.
(10) Rongy, L.; Haugen, K. B.; Firoozabadi, A. Mixing from Fickian diffusion and natural convection in binary non-equilibrium fluid phases. *AIChE J.* **2012**, *58*, 1336–1345.
(11) Almarcha, C.; Trevelyan, P. M. J.; Grosfils, P.; De Wit, A. Chemically driven hydrodynamic instabilities. *Phys. Rev. Lett.* **2010**, *104*, 044501.
(12) Almarcha, C.; R'Honi, Y.; De Decker, Y.; Trevelyan, P. M. J.; Eckert, K.; De Wit, A. Convective mixing induced by acid-base reactions. *J. Phys. Chem. B* **2011**, *115*, 9739–9744.

(13) Trevelyan, P. M. J.; Almarcha, C.; De Wit, A. Buoyancy-driven instabilities of miscible two-layer stratifications in porous media and Hele-Shaw cells. *J. Fluid Mech.* **2011**, *670*, 38−65.
(14) Fernandez, J.; Kurowski, P.; Petitjeans, P.; Meiburg, E. Density-driven unstable flows of miscible fluids in a Hele-Shaw cell. *J. Fluid Mech.* **2002**, *451*, 239−260.
(15) Wylock, C.; Dehaeck, S.; Cartage, T.; Colinet, P.; Haut, B. Experimental study of gas-liquid mass transfer coupled with chemical reactions by digital holographic interferometry. *Chem. Eng. Sci.* **2011**, *66*, 3400−3412.
(16) Aboudheir, A.; Tontiwachwuthikul, P.; Chakma, A.; Idem, R. Kinetics of the reactive absorption of carbon dioxide in high CO_2-loaded, concentrated aqueous monoethanolamine solutions. *Chem. Eng. Sci.* **2003**, *58*, 5195−5210.
(17) Vas Bhat, R. D.; Kuipers, J. A. M.; Versteeg, G. F. Mass transfer with complex chemical reactions in gas-liquid systems: two-step reversible reactions with unit stoichiometric and kinetic orders. *Chem. Eng. J.* **2000**, *76*, 127−152.
(18) Danckwerts, P. V. *Gas-Liquid Reactions*; McGraw-Hill: New York, 1970.
(19) Bird, R. B.; Stewart, W. E.; Lightfoot, E. N. *Transport Phenomena*, 2nd ed.; John Wiley & Sons: New York, 2002.
(20) Gondret, P.; Rabaud, M. Shear instability of two-fluid parallel flow in a Hele-Shaw cell. *Phys. Fluids* **1997**, *9*, 3267−3274.
(21) Ruyer-Quil, C. Inertial corrections to the Darcy law in a Hele-Shaw cell. *C. R. Acad. Sci. Paris IIB Mech.* **2001**, *329*, 337−342.
(22) Martin, J.; Rakotomalala, N.; Salin, D. Gravitational instability of miscible fluids in a Hele-Shaw cell. *Phys. Fluids* **2002**, *14*, 902−905.
(23) Wylock, C.; Dehaeck, S.; Rednikov, A.; Colinet, P. Chemo-hydrodynamical instability created by CO_2 absorption in an aqueous solution of $NaHCO_3$ and Na_2CO_3. *Microgravity Sci. Technol.* **2008**, *20*, 171−175.

SUPPORTING INFORMATION

Nonmonotonic Rayleigh-Taylor Instabilities Driven by Gas-Liquid CO_2 Chemisorption

C. Wylock, A. Rednikov, B. Haut, and P. Colinet

Université Libre de Bruxelles (ULB), Transfers, Interfaces and Processes (TIPs), av. F.D. Roosevelt 50, CP 165/67, 1050 Brussels, Belgium

For gas A absorption into an aqueous solution of B and C accompanied by an irreversible chemical reaction $A + B \to C$, the following reaction-diffusion formulation can be considered as standard:

$$\partial_t[A] = \mathbb{D}_A\, \partial_{zz}[A] - k[A][B]\,, \tag{S.1}$$

$$\partial_t[B] = \mathbb{D}_B\, \partial_{zz}[B] - k[A][B]\,, \tag{S.2}$$

$$\partial_t[C] = \mathbb{D}_C\, \partial_{zz}[C] + k[A][B]\,, \tag{S.3}$$

$$[A] = [A]_f\,, \quad \partial_z[B] = 0\,, \quad \partial_z[C] = 0 \qquad \text{at } z = 0\,, \tag{S.4}$$

$$[A] = 0\,, \quad [B] = [B]_0\,, \quad [C] = [C]_0 \qquad \text{as } z \to +\infty\,. \tag{S.5}$$

Here $[A]_f$ is the interfacial concentration of A (the saturation concentration in contact with a gas A atmosphere, e.g. as given by Henry's law) and k is the reaction rate coefficient. The second and third conditions (S.4) stand for non-penetration of the corresponding species through the interface. We note that in our case the bulk concentration of B is typically much higher than that of the dissolved gas A at the interface (several hundreds versus some tens of mol/m^3). Thus, a relation

$$[A]_f \ll [B]_0 \tag{S.6}$$

will be implied throughout.

Now if we are speaking of an *instantaneous* reaction, what is going here is well described in textbooks, see e.g. Bird et al.[19] Namely, the reaction occurs just in a plane parallel to the interface and located at a certain well-defined distance from the latter. Both A and B are totally consumed at this

plane and cannot coexist elsewhere due to the instantaneous character of the reaction. In particular, $[A] = 0$ below the plane, whereas $[B] = 0$ between the plane and the interface. In view of (S.6), this plane is actually situated sufficiently close to the interface in our case, so that at a global scale we may not distinguish the two. In this way, we arrive at an instantaneous *interfacial* chemical reaction and hence the formulation used in the present study.

On the other hand, we note that what is discussed above is in fact already an extreme version of an instantaneous reaction, with an "unconditionally large" kinetic coefficient k. In particular, the reaction zone is supposed to be much narrower (hence a "plane") than even its distance to the interface, which is also small on account of (S.6). In reality, however, one does not need so strong assumptions for the validity of the simplified chemical reaction model we rely upon here: the reaction zone, while staying narrow may well be allowed to extend up to the interface. We shall illustrate this by approaching the problem from the opposite end: the reaction will still be considered fast in an appropriate sense, but no assumptions on its instantaneous character will a priori be made.

Namely, the reaction is considered fast with respect to diffusion at the length scale l_{ref} of interest, which can here be just the boundary-layer thickness at the onset of the Rayleigh-Taylor instability. In other words, as it can be conjectured e.g. from the form of the reaction and diffusion terms of Eq. (S.1) with $z \sim l_{\mathrm{ref}}$ and $[B] \sim [B]_0$,

$$k[B]_0 \gg \mathbb{D}_A / l_{\mathrm{ref}}^2 \,. \tag{S.7}$$

If so, the reaction occurs only in a zone with $z \sim (\mathbb{D}_A / k[B]_0)^{1/2}$, where the reaction and diffusion effects are of the same order of magnitude and which is narrow at the global scale $z \sim l_{\mathrm{ref}}$. Outside of this zone, at $z \sim l_{\mathrm{ref}}$, we have $[A] = 0$ (we shall see shortly that $[A]$ decays exponentially away from the reaction zone), and the reaction terms vanish in Eqs. (S.2) and (S.3) to yield simply

$$\partial_t [B] = \mathbb{D}_B \, \partial_{zz} [B] \,, \tag{S.8}$$

$$\partial_t [C] = \mathbb{D}_C \, \partial_{zz} [C] \,. \tag{S.9}$$

In the narrow reaction zone $z \sim (\mathbb{D}_A / k[B]_0)^{1/2}$, on the other hand, Eqs. (S.1)–(S.3) become quasi-stationary on the time scale $l_{\mathrm{ref}}^2 / \mathbb{D}_A$:

$$0 = \mathbb{D}_A \, \partial_{zz} [A] - k[A][B] \,, \tag{S.10}$$

$$0 = \mathbb{D}_B \, \partial_{zz} [B] - k[A][B] \,, \tag{S.11}$$

$$0 = \mathbb{D}_C \, \partial_{zz} [C] + k[A][B] \,. \tag{S.12}$$

We note that the diffusion coefficients are all considered to be of the same order of magnitude. Given that $[B] \sim [B]_0$ and $[A] \sim [A]_f$, we see on account of (S.6) that should the reaction appear at the leading order in (S.10), it must just be a correction in (S.11) and (S.12). Hence, in particular, $\partial_{zz}[B] = 0$ to leading order. On account of the boundary condition (S.4), this brings to $[B] =$ constant to leading order in the reaction zone. If so, Eq. (S.10) with the boundary condition (S.4) can be solved assuming further a non-singular behavior at infinity (i.e. toward the bulk) to yield

$$[A] = [A]_f \exp\left(-\sqrt{\frac{k[B]}{\mathbb{D}_A}}\, z\right), \tag{S.13}$$

which indeed decays exponentially. To proceed, one needs to account for the influence of the reaction on $[B]$, which comes from calculating the corresponding correction over $[B] =$ constant. However, one can spare a large part of such a calculation by just integrating Eq. (S.11) along z from 0 to infinity with $[B] =$ constant and (S.13) used in the reaction term. On account of the boundary condition (S.4), we obtain

$$\mathbb{D}_B \partial_z [B]\Big|_{z\to+\infty} = [A]_f \sqrt{k\mathbb{D}_A[B]}\,. \tag{S.14}$$

The matching condition with the main bulk $z \sim l_{\rm ref}$ can symbolically be written as

$$\partial_z [B]\Big|_{(k[B]_0/\mathbb{D}_A)^{1/2} z\to+\infty} = \partial_z [B]\Big|_{z/l_{\rm ref}\to 0}\,, \tag{S.15}$$

implying an overlap in an intermediate zone, where $(k[B]_0/\mathbb{D}_A)^{1/2} z \gg 1$, but $z/l_{\rm ref} \ll 1$, which is clearly possible in view of (S.7). The left-hand side in (S.14) must actually be understood as the one in (S.15). Using (S.15) in (S.14) and taking into account that to leading order the condition for the main zone ($z \sim l_{\rm ref}$) can formally be written directly at $z = 0$, we arrive at

$$\mathbb{D}_B \partial_z [B] = [A]_f \sqrt{k\mathbb{D}_A[B]} \qquad \text{at } z = 0\,. \tag{S.16}$$

A similar boundary condition, now proceeding from (S.12), can be derived for $[C]$:

$$\mathbb{D}_C \partial_z [C] = -[A]_f \sqrt{k\mathbb{D}_A[B]} \qquad \text{at } z = 0\,,$$

which is better to be combined with (S.16) to yield

$$\mathbb{D}_B \partial_z [B] = -\mathbb{D}_C \partial_z [C] \qquad \text{at } z = 0\,. \tag{S.17}$$

Thus, the problem in the main bulk is reduced on account of (S.6) and (S.7) to the one with an effective interfacial chemical reaction, emerging

de facto in the boundary condition (S.16), and with no reaction in the bulk equations (S.8) and (S.9). The other interface boundary condition, given by (S.17), also has a clear physical meaning: the consumption of B in this interfacial reaction is equal to the production of C. The boundary conditions as $z \to +\infty$ are still given by (S.5) for $[B]$ and $[C]$.

The interfacial reaction (S.16) is generally of a finite rate. On the other hand, it can be seen that an instantaneous one can thereof be obtained as a limiting case under the assumption

$$\mathbb{D}_B[B]_0/l_{\mathrm{ref}} \ll [A]_f\sqrt{k\mathbb{D}_A[B]_0}\,, \tag{S.18}$$

which on account of (S.6) and $\mathbb{D}_B \sim \mathbb{D}_A$ is a stronger condition than just (S.7). In this limit, the boundary condition (S.16) turns into

$$[B] = 0 \qquad \text{at } z = 0\,. \tag{S.19}$$

Thus, the simplified chemical reaction formulation used in the present study is fully recovered. In the framework of a full standard model (S.1)–(S.5), its validity conditions are given by (S.6) and (S.18).

Note that sufficiently deep into the limit (S.18), the reaction zone developments like (S.13) cease to be valid as actually obtained under the assumption $[B] \gg [A]$ (after all, Eq. (S.13) becomes meaningless for $[B] \to 0$ with a vanishing exponent). Then a different approximation scheme, suitable for the case $[A] \sim [B] \ll [B]_0$, must be adopted for the reaction zone, which for even higher values of k would permit recovering the reaction-in-the-plane limit we started with in the present model. Anyhow, all such details are already immaterial for our goals here, since the boundary condition (S.19) (instantaneous interfacial chemical reaction) holds anyway to leading order for any such transformations of the reaction zone.

Finally, we note that the present developments also hold in the presence of advective contributions in the reaction-diffusion equations, provided that the reaction zone is thin enough for the locally defined Peclet numbers to be small (even if the global ones are not).

References

[19] Bird, R. B.; Stewart, W. E.; Lightfoot, E. N. *Transport phenomena*, 2nd ed.; John Wiley & Sons, 2002.